Fast, Air-Stable Infrared Photodetectors based on Spray-Deposited Aqueous HgTe Quantum Dots

*Mengyu Chen, Hui Yu, Stephen V. Kershaw, Haihua Xu, Shuchi Gupta, Frederik Hetsch, Andrey L. Rogach, and Ni Zhao**

The ability to detect near-infrared and mid-infrared radiation has spawned great interest in colloidal HgTe quantum dots (QDs). In contrast to the studies focused on extending the spectral range of HgTe QD devices, the temporal response, another figure of merit for photodetectors, is rarely investigated. In this work, a single layer, aqueous HgTe QD based photoconductor structure with very fast temporal response (up to 1 MHz 3 dB bandwidth) is demonstrated. The device is fabricated using a simple spray-coating process and shows excellent stability in ambient conditions. The origin of the remarkably fast time response is investigated by combining light intensity-dependent transient photocurrent, temperature-dependent photocurrent, and field-effect transistor (FET) measurements. The charge carrier mobility, as well as the energy levels and carrier lifetimes associated with the trap states in the QDs, are identified. The results suggest that the temporal response is dominated by a fast bimolecular recombination process under high light intensity and by a trap-mediated recombination process at low light intensity. Interestingly, it was found that the gain and time response of aqueous HgTe QD-based photoconductors can be tuned by controlling the QD size and surface chemistry, which provides a versatile approach to optimize the photodetectors with selectable sensitivity and operation bandwidth.

1. Introduction

Near infrared and short wave infrared (NIR-SWIR) photodetectors offer promising applications in passive night vision,[1] bio-diagnostics,[2] and optical communication.[3] Current NIR-SWIR technologies are expensive, as the manufacturing process relies on costly, size-limited epitaxial growth of compound semiconductors on rigid crystalline substrates.[4] Contrastingly narrow-bandgap colloidal semiconductor quantum dots (QDs) offer opportunities for manufacturing low-cost, large-area high performance photodetectors due to their low-temperature solution-processibility as well as the tunability of their electronic structures.

QD based photoconductors are attractive as photodetector structures for commercial applications since they can be fabricated using high-throughput processes such as inkjet-printing[5] and spray-coating,[6] and are easily integrated with conventional read-out integrated circuits. The detectivity (D*) of QD photoconductors has exceeded 10^{12} Jones, which rivals conventional inorganic technologies. This performance was achieved largely through the engineering of QD trap states in order to maximize the photoconductive gain. On the other hand, QD photoconductors suffer from a slow temporal response.[7] For instance, Konstantatos et al. reported a lead sulfide (PbS) QD based photoconductor with a remarkable detectivity (D*) of ≈10^{13} Jones;[8] however, the 3 dB bandwidth of the photoconductor is limited to 20 Hz, much lower compared to that photodiodes made with similar QD materials.[9,10] Although the slow temporal response of the photoconductors can be improved by modifying the surface chemistry of the QDs, it is still limited by the long lifetime (~ms) of the fastest trap state[11,12] present in PbS QD systems. Nanocrystalline HgTe is another promising infrared material, with a broad spectral tuneability from the NIR to the mid-IR.[14–16] The first photoconductor with organic-based HgTe QDs (grown in organic solvents, etc.) showed spectral sensitivity up to 3 μm,[5] and this record was subsequently improved to 5 μm by Keuleyan et al.[17] While these studies focused on extending the spectral range of HgTe QD devices, their temporal response (or the bandwidth), which is another important figure of merit for photodetectors, is rarely investigated.[18,19]

In this work, we demonstrated a single layer, photoconductor structure based on aqueous HgTe QDs with a very fast temporal response (up to 1 MHz 3 dB bandwidth). The device was fabricated by a simple spray-coating process and showed excellent stability under ambient conditions. The origin of the remarkably fast time response is investigated by combining light intensity-dependent transient photocurrent, temperature-dependent photocurrent, and field-effect transistor (FET) measurements. The results reveal the temporal response is dominated by a fast bimolecular recombination process under high

M. Chen, H. Yu, Dr. H. Xu, Prof. N. Zhao
Department of Electronic Engineering
The Chinese University of Hong Kong
New Territories, Hong Kong
E-mail: nzhao@ee.cuhk.edu.hk
Dr. S. V. Kershaw, S. Gupta, F. Hetsch, Prof. A. L. Rogach
Department of Physics and Materials Science
and Centre for Functional Photonics (CFP)
City University of Hong Kong
Hong Kong S.A.R.

DOI: 10.1002/adfm.201301006

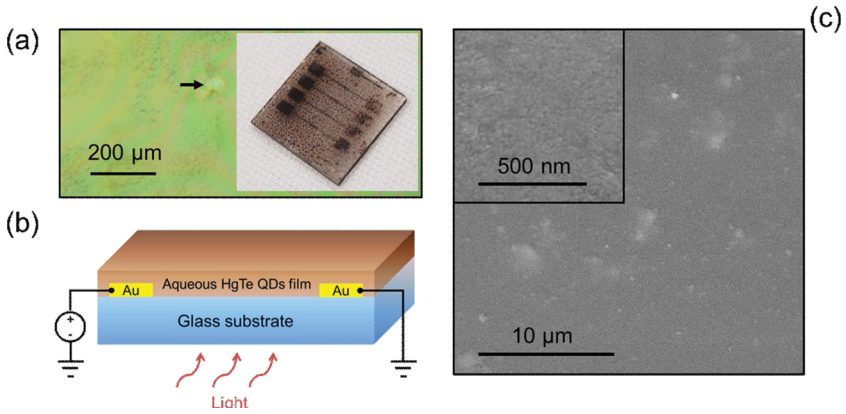

Figure 1. Device structure and surface morphology. a) Optical image of the HgTe QD film after a few passes of spray-coating. The arrow highlights some of the substrate regions that are uncovered with QDs, which can be filled up in the following spray passes. Inset: image of four spray-coated photoconductors with different W/L ratios on one chip. b) Device structure. c) SEM images of the same film in (a) on two length scales.

light intensity illumination and by a trap-mediated recombination process at low light intensities. The lifetimes of the trap states in the HgTe QD system are much lower than those in PbS QDs.[11,12] The gain and time response of aqueous HgTe QD based photoconductor can be tuned by controlling the QD size and surface chemistry.

2. Results and Discussion

The HgTe QDs used in this study were directly synthesized in aqueous solutions via a room temperature reaction between $Hg(ClO_4)_2$ and H_2Te gas in the presence of 1-thioglycerol (TG).[20,21] The as-prepared aqueous HgTe QD solutions contain an excess of ions such as Na^+ and Hg^{2+}, which can largely degrade the device performance.[22] To remove them, the HgTe QDs were precipitated from solution with methanol and then re-dissolved in deionized water before the spray coating process. We found that this purification process is key to the fast operation of the QD photoconductors. A comparison of the photocurrent and the response speed before and after purification is provided in the Supporting Information, Figure S1.

Unlike organic-based QDs with long ligands (for example, dodecanenthiol), the aqueous QDs are capped with very short ligands and stabilized in water via electrostatic interaction,[23] obviating the need for ligand exchange otherwise necessary for reasonable carrier mobility in electronic or photoelectric devices. This therefore allows a less laborious and higher throughput manufacturing process. However, the poor volatility and large surface tension of water as well as the low solute concentration make it difficult to form a continuous and thick enough QD film via conventional fabrication techniques such as spin-coating or drop-casting. We therefore chose a modified spray-coating technique[6,24] to layer-by-layer deposit the HgTe QDs. In particular, we kept the substrate temperature at around 45 °C and introduced a gas flow above the substrate surface to control the drying process. These conditions are critical to reduce the coffee-ring effect (uneven, patterned drying).[25] The optical image in **Figure 1**a shows a continuous QD film formed after a few passes of spray-coating; the small uncovered regions can be filled up in the following passes. The microscopic morphology of the QD film is revealed in the SEM images in Figure 1c. No micro- or nanoscale cracks are observed in the film. The visible particles in the film are most likely formed by QD aggregation. To fabricate the photoconductors (as shown in Figure 1b), the gold interdigitated electrodes are first deposited on the glass substrates by thermal evaporation of the conductor followed by photolithography. Before spray-coating, the substrates are treated with an oxygen plasma for five minutes. For all the devices presented here, the thickness of the QD layers is in the range of 150 to 200 nm. The diameter of the QDs is about 3 nm, corresponding to a photoluminescence (PL) wavelength of around 1300 nm.

Figure 2a,b show the room temperature spectral responsivity, internal quantum efficiency (IQE) spectrum, and the detectivity wavelength dependence of the devices ($W = 15$ mm, $L = 3$ μm), characterized using the methods described elsewhere.[26] It can be seen that the responsivity and detectivity spectra correlate well the absorption spectrum of the QD films (Figure S2, Supporting Information). The value of the IQE is larger than 100% (ranging from 150% to 1000%), which demonstrates the photoconductive gain of the device. The detectivity D* is larger than 10^{10} cm $Hz^{1/2}$ W^{-1} below 1100 nm. We note that both the IQE and D* are lower than PbS QD based photoconductors with a similar device structure.[27] This is mainly due to the fast recombination of photogenerated charge carriers, which will be discussed later. Figure 2c shows the normalized photocurrent as a function of the modulation frequency. The 3 dB bandwidth of the device can reach more than 1 MHz under sufficiently high illumination intensities (≥800 mW cm^{-2}). This value is much higher than that of the single layer PbS QD photoconductors (≈10 kHz) and close to the record currently held for organic/QD hetero-junction photodetectors (≈2 MHz) measured under the same illumination level.[27] The waveform in Figure 2d demonstrates the response of the device to the light source modulated at 100 kHz frequency. The square-waveform is conserved well with small distortion.

To understand the origin of the fast response of the HgTe QD photoconductors, we first measured the photocurrent under different light intensities (**Figure 3**a). A power law dependence of the normalized photocurrent (i_{norm}) on the light intensity (I), that is, $i_{norm} \propto I\alpha$, is observed. Here α (=0.42) is close to 0.5, indicating that the dominant loss mechanism of the photocurrent is bimolecular recombination.[28] To correlate this result with the temporal response of the QD photoconductors, we measured the transient photocurrent decays after removal of the incident light. The results are plotted in Figure 3b for different light intensities. We found that following the initial fast bimolecular recombination process (<1 μs) the excess charge carriers are annihilated via trap-mediated recombination. The lifetime of the trapped carriers can be estimated by fitting the tail of the decay curves with three exponential functions, which

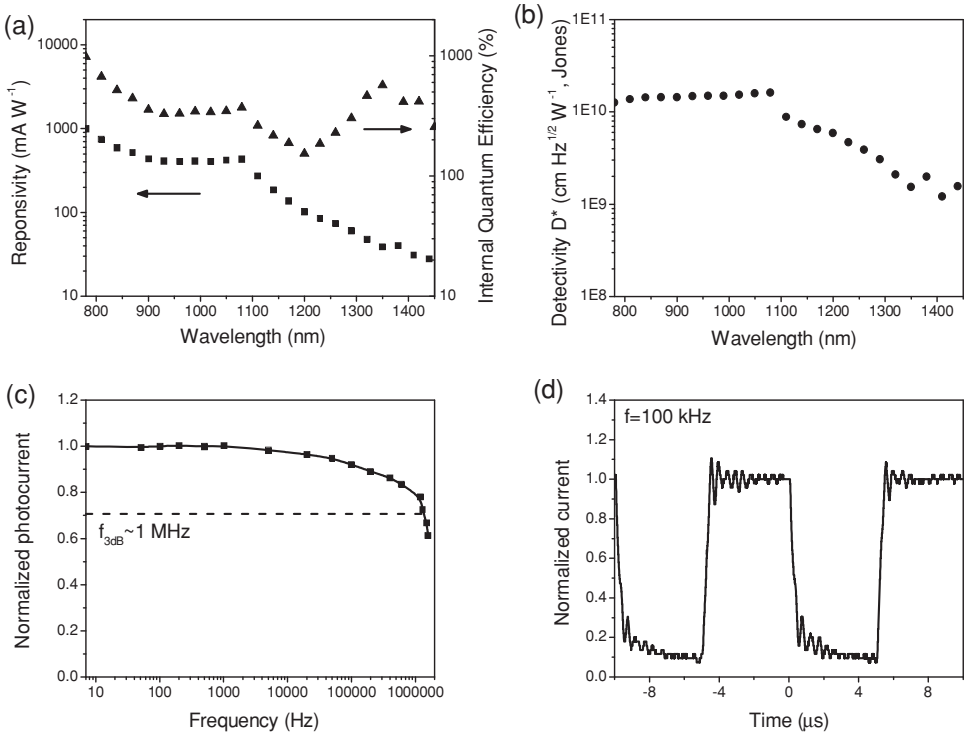

Figure 2. Spectral and frequency response of a typical aqueous HgTe QD photoconductor (W = 15 mm, L = 3 μm). a) Responsivity and IQE as a function of wavelength (295 K, bias = 60 V). b) Detectivity as a function of wavelength (295 K, bias = 15 V). c) Frequency dependence of the photocurrent illuminated by a square-wave modulated 8 mW, 635 nm laser (295 K, bias = 5 V, I = 800 mW cm^{-2}). d) The normalized photocurrent transient response of the 100 kHz point in (c).

yields the time constants $\tau_1 \approx 1.8$ μs, $\tau_2 \approx 80$ μs, and $\tau_2 \approx 2$ ms. Under high light intensities, the bimolecular recombination and fast trap states dominate the photocurrent decay, leading to rapid response of the device to incident light. Under low light intensities, on the other hand, the photogenerated charge carriers mostly reside in deep traps and recombine slowly. Accordingly, the 3 dB bandwidth drops from 1 MHz to 1 kHz when the light intensity is reduced by three orders of magnitude (the

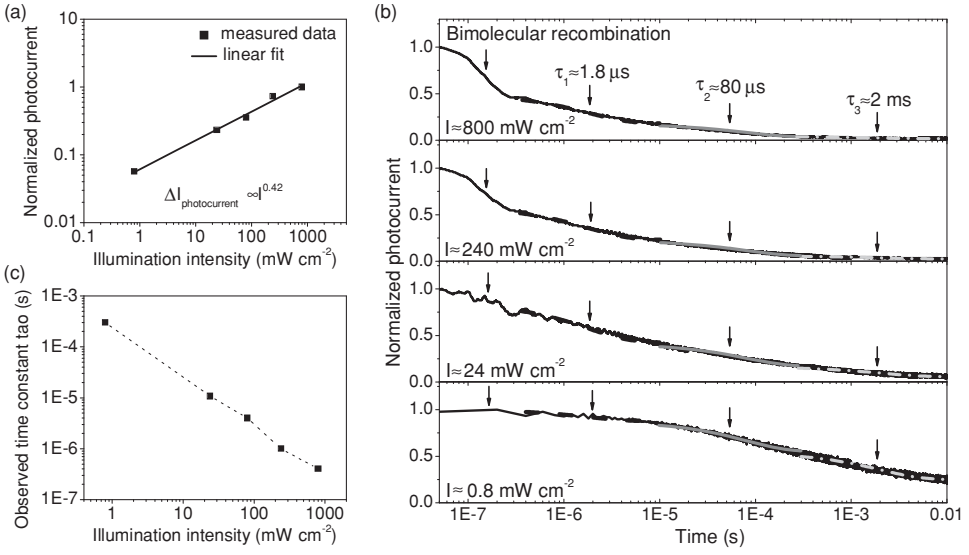

Figure 3. Light intensity dependent measurements of an aqueous HgTe photodetector. a) The normalized photocurrent under different illumination levels and fitted curve. b) Light intensity dependent transient decays under different illumination levels. The decay slopes due to recombination and different trap states are marked by arrows, respectively. c) Observed time constants (the time needed to fall to the e^{-1} of the original amplitude in the decay tail) of the photocurrent decay versus illumination levels.

responsivity is greatly increased at the same time as shown in Figure S3, Supporting Information). We note that even at the lowest light intensity (≈0.8 mW cm^{-2}) the time constant of the HgTe QD photoconductor is about 300 μs (Figure 3c), which is much shorter than that of PbS QD devices (7 ms ± 3 ms) with similar structures and at comparable illumination levels.[27] This large difference in time constants should originate from the different chemical nature of the trap states in each case, which could be identified via chemical and spectroscopic analysis.[11] This research is currently underway. The trap density can be estimated based on the transient photocurrent response under 0.8 mW cm^{-2} illumination, where the decay curve is dominated by the recombination of the trapped charges. Assuming one charge per trap state, the total number of trap states is the integral of current over time. The number of QDs can be estimated using the close-packing model.[13] Therefore, the calculated trap density is about 0.25 traps-per-QD (detailed calculation is described in the Supporting Information).

To further understand the distribution of trap states within the bandgap of HgTe QDs, we characterized the temperature dependence of the photocurrent using the same method applied to PbS QD systems.[12] In photoconductors, the photocurrent is defined as:

$$I_P = P\eta q\tau_c/h\nu\tau_t = P\eta q\tau_c\mu E/h\nu L \quad (1)$$

where P is the impinging optical power, η is the quantum efficiency, τ_c is the carrier lifetime, τ_t is the transit time, and E is the electric field across the electrode spacing L. FET measurements, which will be presented later on, suggest that there are large numbers of electron traps in the QD films, and that hole transport should dominate the current conduction. Accordingly, we can take the values of the hole mobility and the electron trap lifetime for μ and τ_c in the above equation. To characterize the temperature dependence of these two parameters, we measured both the dark current and photocurrent under high and low illumination levels in the temperature range from 320 K to 170 K (Figure S4, Supporting Information). The photocurrent can be considered as a trade-off between two processes: thermally activated hole transport and thermally accelerated de-trapping of electrons. When the temperature decreases, the hole mobility will decrease, thus lowering both the dark current and the photocurrent. On the other hand, the trapped electrons will be gradually "frozen" in the trap states, providing longer trapping time and therefore increasing the photocurrent. To decouple the effects of these two processes, we first use the dark current to extrapolate the temperature dependence of the hole mobility since the dark current is dominated by hole transport. Then, by factoring out the effective mobility from the photocurrent, we obtain a physical value that depends only on the lifetime of trapped electrons. Since this value decreases with τ_c at high temperatures (above 250 K), it is referred as photocurrent quenching.[12] For a system with single-level traps, the photocurrent quenching rate is expected to be proportional to $\exp(-\Delta E/kT)$, where ΔE is the depth of the trap states from the conduction band. Thus, the slope of the natural logarithm of the photocurrent quenching versus the inverse of the temperature would correspond to the depth of the trap states. **Figure 4**a shows the photocurrent quenching curves measured under two different illumination levels. Based on the results of the transient photocurrent measurement (Figure 3a), we fit the data by assuming three trap levels, corresponding to three different lifetimes of trapped carriers. Both photocurrent quenching curves can be well fitted by setting the trap state levels at 0.33 eV, 0.24 eV, and 0.13 eV, respectively, away from the conduction band edge. We can further correlate this result with the carrier lifetimes obtained from Figure 3a. The temperature dependence of the carrier lifetime is given by:

$$\tau^{-1} = \sigma_n N_c \nu_{th} \exp(-\Delta E/kT) \quad (2)$$

where σ_n is the capture cross-section of the trap, N_c is the density of the states in conduction band, and ν_{th} is the thermal velocity of the carriers.[11] Therefore the energy differences between three trap states can be calculated using the carrier lifetimes obtained from the transient photocurrent measurement:

$$\Delta E_2 - \Delta E_1 = kT\ln(\tau_2/\tau_1) \approx 0.1 \text{ eV}$$
$$\Delta E_3 - \Delta E_2 = kT\ln(\tau_3/\tau_2) \approx 0.08 \text{ eV} \quad (3)$$

This result agrees well with the values of the energy difference calculated from the temperature dependence of the photocurrent quenching, which are around 0.09 eV and 0.11 eV, respectively.

Based on the transient photocurrent decay and the temperature dependence of the photocurrent quenching, we suggest the fast response of the HgTe QD photoconductors is due to the short lifetime of the trapped carriers in HgTe QDs and the relatively low density of the trap states. Additionally, there may be a large number of recombination centers in thiol-capped QDs, which are responsible for the fast bimolecular recombination process as well as the short photoluminescence (PL) decay and low PL efficiency.[29] Although enabling fast temporal response, the aforementioned properties of the trap states in the HgTe QDs limit the photoresponsivity of the QD based photoconductors as the carrier lifetime, which is proportional to the photocurrent, is short. Conversely, high charge carrier mobility should offer high photoconductive gain. In order to

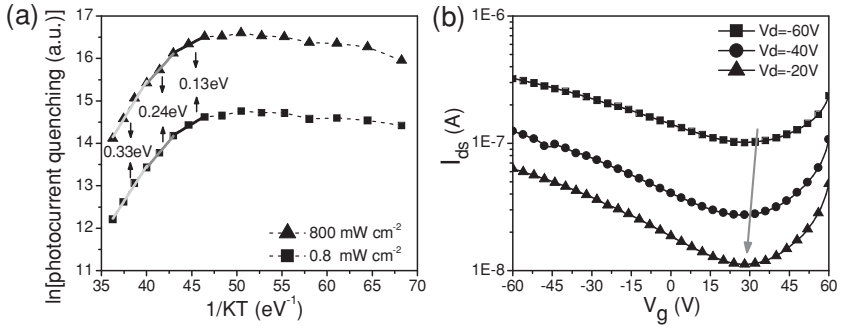

Figure 4. a) Photocurrent quenching as a function of temperature at two illumination levels. Three sensitizing centers with energy depths of ≈0.13 eV, ≈0.24 eV, and ≈0.33 eV from the conduction band gives a reasonable fit for the slopes of the quenching curves in the positive gradient region. b) Transfer characteristics of an aqueous HgTe QD FET (W = 15 mm, L = 20 μm). The turn-off voltage is slightly reduced with decreasing drain voltage as indicated by the arrow.

characterize the charge transport properties of HgTe QD films, we fabricated a bottom-contact bottom-gate FET structure by depositing the QD films on highly doped silicon substrates (used as the gate) with 300 nm SiO_2 dielectric and pre-patterned gold source-drain electrodes. The devices show clear ambipolar behavior, as shown in the transfer curves in Figure 4b. The device appears to be hard to "turn-off" because of the high recombination current in the ambipolar regime. The typical hole and electron mobilities are $\mu_h \approx 5.0 \times 10^{-6}$ cm^2 (V s)$^{-1}$ and $\mu_e \approx 9.0 \times 10^{-7}$ cm^2 (V s)$^{-1}$ respectively. (Detailed calculation is provided with Figure S5,S6 in the Supporting Information.) Besides the mobility difference, we also observe a much higher threshold voltage for the formation of the n-type channel as compared to the p-type channel. This suggests that the deep trap density for electrons is much higher than that for holes. Therefore, we can assume that the electron traps determine the carrier lifetime and evaluate the gain of the photoconductor. The transit time of the hole can be defined by:

$$\tau_t = L^2/(\mu_h \times V) \quad (4)$$

where L is the electrode spacing (3 μm) and V is the applied voltage (60 V). The maximum photoconductive gain is then given by $G = \tau_c/\tau_t \approx 7$, if the carrier lifetime of the deepest trap states is used. The value is comparable with the measured maximum gain (estimated from the IQE shown in Figure 1a).

We observed that the aqueous HgTe QD based photoconductors show good air stability. Even without encapsulation the devices exhibit stable performance after several hours of continuous testing under high illumination levels and under ambient conditions. The longer term stability was also studied, as shown in **Figure 5**. In this case, the device was exposed in the ambient environment for more than one month, during which it was tested every few days. In the first two days, the bandwidth and the photocurrent showed little variation. Starting from the fourth day, the photoresponse became slower, indicating that the density of the trap states in the QDs film was increased, likely due to oxidation. An increase in the trap state density should also increase the photoconductive gain, although this may be compromised by a corresponding increase in the resistivity of the QD films. The photocurrent showed a slight increase after one month, while the 3 dB bandwidth decreased by about an order of magnitude.

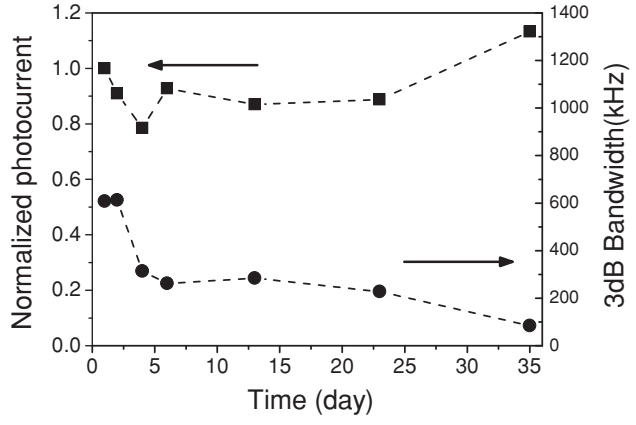

Figure 5. Degradation test of an aqueous HgTe QD photoconductor (W = 15 mm, L = 10 μm). The normalized photocurrent and the 3 dB bandwidth, f_{3dB} (evaluated from the observed time constant τ, where $f_{3dB} = 1/(2\pi\tau)$),[26] of the photoconductor as a function of the exposure time in ambient environments.

Besides oxidation, we found that the size and surface chemistry of the QDs can also greatly affect the gain and transient response. **Figure 6**a shows the comparison of the dark and light current of the devices made with QDs of two different sizes (3.1 nm and 3.7 nm corresponding to the PL wavelengths of 1300 nm and 1600 nm, respectively, of the precursor solutions from which the devices were fabricated). Both the dark and light current of the long wavelength QD devices are at least one-order higher than that of the short wavelength QD devices. For example, under 5 V bias, the photocurrent increases from ≈9×10^{-7} A to ≈6×10^{-6} A, suggesting that the responsivity of the 1600 nm QD device is increased by more than 6 times compared to the 1300 nm device. This result could also explain the high responsivity reported in the 5 μm (spectral response) HgTe QD devices.[17] The temporal response of the 1600 nm QD device increases to 2 μs, as shown in Figure 6b, suggesting the formation of different trap states due to the change in the surface chemistry of the QDs. One can expect that aqueous HgTe QDs will become more conductive but contain slower traps if their size is increased to 7–10 nm (corresponding to mid-infrared PL wavelengths), as already shown for HgTe QDs synthesized in organic solvents with long alkyl chain ligands.[5,17] Therefore there should be a large window to tune the responsivity and bandwidth of the photodetectors by controlling the size and surface chemistry of HgTe QDs.

3. Conclusions

We have demonstrated an aqueous HgTe QD based SWIR photoconductor structure with up to 1 MHz 3 dB bandwidth. The device was fabricated using a simple spray-coating process and showed excellent stability in ambient conditions. The origin of the fast temporal response and the photoconductive gain can be explained by a fast bimolecular recombination process and short lifetimes of the electron trap states in the QD films. Accordingly, these two device parameters can be tuned by controlling the QD size and surface chemistry, which will allow further optimization of the device performance. The findings presented herein not only demonstrate a versatile approach to fabricate QD photodetectors with selectable sensitivity and operation bandwidth, but also shed light on the charge transport and charge recombination mechanism in HgTe QD films. The methodology developed here can be scaled up to produce large-area SWIR photodetector arrays through a low-cost and high-throughput manufacturing process.

4. Experimental Section

Device Fabrication: The gold interdigitated electrodes were fabricated on a glass substrate (Corning 7059) by photolithography, thermal deposition, and lift-off with metal thickness of about 30 nm. The concentration of the aqueous HgTe QDs solution for spray-coating was about 40–50 mg (QD solids) mL^{-1}. The nozzle of the airbrush was

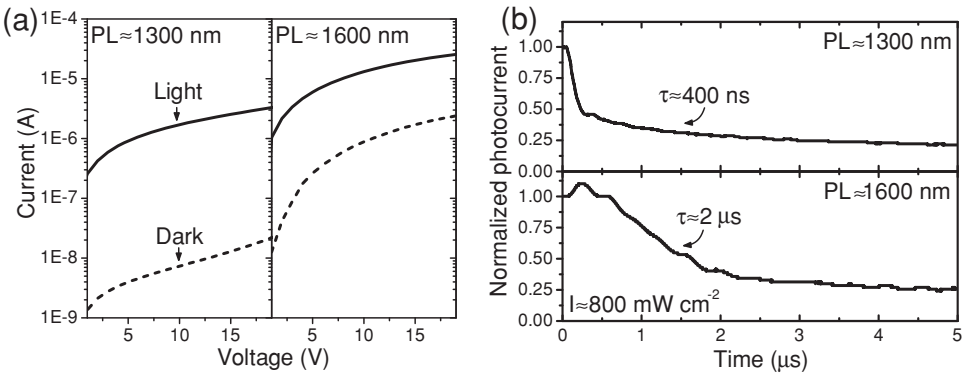

Figure 6. Comparison of a) the photocurrent and b) the photocurrent transient response of aqueous HgTe QD based photoconductors working at short (around 1300 nm) and long wavelength (around 1600 nm) under the same illumination level (the wavelengths here denote the position of the peak photoluminescence of the QD solutions from which the test film devices were fabricated). The observed time constants are marked in (b).

300 nm with a distance to the hotplate around 11 cm. The pressure of both the spraying and blowing gas was 0.5 bar, and the hotplate was set to 45 °C for accelerated drying. After about 50 passes, the thickness of the QD films could reach 150–200 nm.

Characterization: Responsivity and detectivity were measured under monochromatic illumination generated by focusing a 250 W quartz tungsten halogen (QTH) lamp into a Newport 74125 Oriel Cornerstone 260 1/4 m monochromator. The light was optically chopped, with a reference signal provided for a lock-in amplifier to measure the AC photocurrent. A germanium photodetector was used to calibrate the optical power density of the spectrally-resolved output. The optical power density was measured to be about 1 mW cm^{-2} at λ = 800 nm. Both the transmission and the scattered light spectra were measured to obtain the absorption data for IQE calculation. The transmission was measured by a Hitachi U-3501 UV-visible/NIR spectrophotometer, and the scattered light spectrum was measured by a dark-field optical microscope (Olympus BX60) that was coupled to a 100 W QTH lamp, an Acton SpectraPro 2300 monochromator and two charge-coupled device (CCD) cameras. The cameras were thermoelectrically cooled during the measurements (–70 °C for the visible CCD (Si); –100 °C (with liquid nitrogen) for the IR CCD (InGaAs)).

Photocurrent Frequency Dependence and Transient Response: A Newport LQD635-03C laser diode, with square-wave modulation at different frequencies, was used to illuminate the devices. The resulting photocurrent was amplified by a Femto DHPCA-100 High Speed Current Amplifier and measured with a Tektronix TDS 3014C Oscilloscope. The photocurrent decays and all the observed time constants in this study were measured with a pulse repetition frequency of 41 Hz. The photocurrent in the degradation tests was measured under steady state laser illumination.

Temperature-Dependent Photocurrent Measurements: The samples for the temperature-dependent photocurrent measurements were tested under vacuum inside a liquid nitrogen cryostat with 10 K decrements and left to equilibrate 10 min at each temperature level. The light source was the same as for the transient response test.

Notes: The devices were biased by a Keithley 2400 Source Meter in all the tests, except for the current–voltage characteristics, which were measured in a glove-box with a Keithley 2612 Source Meter both in the dark and under illumination from a 20 mW, 780 nm laser diode.

Supporting Information

Supporting Information is available from the Wiley Online Library or from the author.

Acknowledgements

The authors gratefully acknowledge funding from the National Natural Science Foundation of China (Grants No. A.03.13.01401) and the Direct Grant from Chinese University of Hong Kong (Grant no. 4055012). This work was also supported by an Applied Research Grant of City University of Hong Kong (9667067), and by a grant from the Research Grants Council of the Hong Kong S. A. R., China (project CityU 102412).

Received: March 21, 2013
Revised: April 17, 2013
Published online: June 20, 2013

[1] J.-E. Källhammer, *Nat. Photonics* **2006**, *sample issue*, 12.
[2] S. Kim, Y. T. Lim, E. G. Soltesz, A. M. D. Grand, J. Lee, A. Nakayama, J. A. Parker, T. Mihaljevic, R. G. Laurence, D. M. Dor, L. H. Cohn, M. G. Bawendi, J. V. Frangioni, *Nat. Biotechnol.* **2004**, *22*, 93.
[3] J. M. Kahn, J. R. Barry, *Wireless Infrared Communications. Proc. IEEE* **1997**, *85*, 265
[4] A. Rogalski, *Infrared Phys. Technol.* **2011**, *54*, 136.
[5] M. Böberl, M. V. Kovalenko, S. Gamerith, E. J. W. List, W. Heiss, *Adv. Mater.* **2007**, *19*, 3574.
[6] V. A. Akhavan, B. W. Goodfellow, M. G. Panthani, D. K. Reid, D. J. Hellebusch, T. Adachi, B. A. Korgel, *Energy Environ. Sci.* **2010**, *3*, 1600.
[7] G. Konstantatos, E. H. Sargent, *Infrared Phys.Technol.* **2011**, *54*, 278.
[8] G. Konstantatos, I. Howard, A. Fisher, S. Hoogland, J. Clifford, E. Klem, L. Levina, E. H. Sargent, *Nature* **2006**, *442*, 180.
[9] J. P. Clifford, G. Konstantatos, K. W. Johnston, S. Hoogland, L. Levina, E. H. Sargent, *Nat. Nanotechnol.* **2008**, *4*, 40.
[10] B. N. Pal, I. Robel, A. Mohite, R. Laocharoensuk, D. J. Werder, V. I. Klimov, *Adv. Funct. Mater.* **2012**, *22*, 1741.
[11] G. Konstantatos, L. Levina, A. Fisher, E. H. Sargent, *Nano Lett.* **2008**, *8*, 1446.
[12] G. Konstantatos, E. H. Sargent, *Appl. Phys. Lett.* **2007**, *91*, 173505.
[13] T. P. Osedach, N. Zhao, T. L. Andrew, P. R. Brown, D. D. Wanger, D. B. Strasfeld, L.-Y. Chang, M. G. Bawendi, V. Bulovic, *ACS Nano* **2012**, *6*, 3121.
[14] A. L. Rogach, S. V. Kershaw, M. Burt, M. Harrison, A. Kornowski, A. Eychmüller, H. Weller, *Adv. Mater.* **1999**, *11*, 552.
[15] S. V. Kershaw, M. Harrison, A. L. Rogach, A. Kornowski, *IEEE J. Sel. Top. Quantum Electron.* **2000**, *6*, 534.

[16] M. V. Kovalenko, E. Kaufmann, D. Pachinger, J. Roither, M. Huber, J. Stangl, G. Hesser, R. Schäffler, W. Heiss, *J. Am. Chem. Soc.* **2006**, *128*, 3516.
[17] S. Keuleyan, E. Lhuillier, V. Brajuskovic, P. Guyot-Sionnest, *Nat. Photonics* **2011**, *5*, 489.
[18] S. H. Im, H.-J. Kim, S. W. Kim, S.-W. Kim, S. I. Seok, *Nanoscale* **2012**, *4*, 1581.
[19] G. I. Koleilat, L. Levina, H. Shukla, S. H. Myrskog, S. Hinds, A. G. Pattantyus-Abraham, E. H. Sargent, *ACS Nano* **2008**, *2*, 833.
[20] S. Gupta, O. Zhovtiuk, A. Vaneski, Y.-C. Lin, W.-C Chou, S. V. Kershaw, A. L. Rogach, *Part. Part. Syst. Charact.* **2013**, *30*, 346.
[21] S. V. Kershaw, A. S. Susha, A. L. Rogach, *Chem. Soc. Rev.* **2013**, *42*, 3033.
[22] H. Kim, K. Cho, H. Song, B. Min, J.-S. Lee, *Appl. Phys. Lett.* **2003**, *83*, 4619.
[23] N. Gaponik, A. L. Rogach, *Phys. Chem. Chem. Phys.* **2010**, *12*, 8685.
[24] S. F. Tedde, J. Kern, T. Sterzl, J. Fürst, P. Lugli, O. Hayden, *Nano Lett.* **2009**, *9*, 980.
[25] E. Tekin, P. J. Smith, S. Hoeppener, A. M. J. van den Berg, A. S. Susha, A. L. Rogach, J. Feldmann, U. S. Schubert, *Adv. Funct. Mater.* **2007**, *17*, 23.
[26] E. L. Dereniak, G. D. Boreman, *Infrared Detectors and Systems*, John Wiley and Sons, Inc., New York **1996**, Ch. 5, 6, 8.
[27] T. P. Osedach, N. Zhao, S. M. Geyer, L.-Y. Chang, D. D. Wanger, A. C. Arango, M. C. Bawendi, V. Bulovic, *Adv. Mater.* **2010**, *22*, 5250.
[28] R. H. Bube, *Photoconductivity of Solids*, John Wiley and Sons, Inc., New York **1960**, Vol. *3*.
[29] A. M. Kapitonov, A. P. Stupak, S. V. Gaponenko, E. P. Petrov, A. L. Rogach, A. Eychmüller, *J. Phys. Chem. B* **1999**, *103*, 10109.